CrossMark

**RESEARCH PAPER**

# Isolation and retrieval of circulating tumor cells on a microchip with double parallel layers of herringbone structure

Peng Xue[1] · Lei Zhang[2] · Jinhong Guo[3,4] · Zhigang Xu[1] · Yuejun Kang[1]

**Abstract** Isolation of the extremely rare circulating tumor cells (CTCs) from peripheral blood has become an effective tool for monitoring and staging tumor development, based on which the therapeutic efficacy can be evaluated. Many techniques have been developed for CTC isolation and enumeration. However, isolation and detection of CTCs with high sensitivity remains a challenging work, and there still exists an urgent demand to retrieve tumor cells after isolation for further molecular and cellular analyses. Herein, we report a dual-functional microchip with double parallel layers of herringbone structure. CTC isolation and retrieving can be simply achieved based on the reversible conjugation with anti-EpCAM modified on the interior channel surface. Specifically, two major strategies were engaged to improve the CTC isolation based on the synergistic effect of significantly increased functional surface area and local microvortex mixing. This approach could achieve CTC isolation efficiency of 75% on average and the detection limit down to 10 cells mL$^{-1}$. Furthermore, CTC retrieving rate was found at 73.4%. Therefore, the present method has a good potential for quantitation and retrieving CTCs with high efficiency for precise cancer diagnosis and subsequent cellular and molecular analyses.

## 1 Introduction

Circulating tumor cells (CTCs) are derived from primary tumor mass and enter the peripheral blood circulation, which is the major cause of metastatic tumor (Zetter 1998; Bernards and Weinberg 2002; Norton and Massague 2006) and responsible for the mortality of patients based on clinical data (Valastyan and Weinberg 2011). The number of CTCs per unit volume of peripheral blood works as a critical index to stage the progress of metastasis, which is directly related to the survival of patients with carcinomas (Giuliano et al. 2014; Devriese et al. 2012; Tsai et al. 2016; Barok and Szollosi 2011). Additionally, the frequency of CTCs also serves as a complementary indicator to monitor the efficacy of cancer therapeutics (Li et al. 2016; Gorges and Pantel 2013). Therefore, characterization of CTCs in peripheral blood has become a minimal invasive tool in liquid biopsy for early diagnosis of cancer and evaluation of cancer therapy (Balic et al. 2013; Yu et al. 2014).

However, the extremely low occurrence of CTCs in the peripheral blood (1–10 CTCs mL$^{-1}$) makes the enrichment and enumeration of CTCs a highly challenging task (den Toonder 2011; Alix-Panabieres and Pantel 2014). There exists an urgent demand to precisely isolate CTCs with high sensitivity and specificity. Currently, microfluidic lab-on-a-chip devices provide attractive opportunities for CTC capture and characterizations, owing to many advantages of tiny sample volume, rapid processing, low cost, and

✉ Yuejun Kang
yjkang@swu.edu.cn

1 Faculty of Materials and Energy, Institute for Clean Energy and Advanced Materials, Southwest University, 2 Tiansheng Road, Chongqing 400715, People's Republic of China

2 School of Chemical and Biomedical Engineering, Nanyang Technological University, 62 Nanyang Drive, Singapore 637459, Singapore

3 University of Electronic Science and Technology of China, 2006 Xiyuan Ave, Chengdu 611371, People's Republic of China

4 Microfluidic POCT Research and Development Centre, Sichuan LaYa Micro Technology Co. Ltd., Chengdu 610041, People's Republic of China

point-of-care multi-detection (van de Stolpe et al. 2011). To date, the majority of current techniques developed for CTC isolation are specifically based on either physical properties (e.g., size, density, deformability, and dielectric property) or biological properties (specific surface protein expression). For those applying physical properties, size- and deformability-based methods (Hosokawa et al. 2009; Sun et al. 2012; Tang et al. 2014; Wang et al. 2015; Warkiani et al. 2016) and label-free dielectrophoresis methods (Gascoyne and Shim 2014; Morimoto et al. 2015; Alazzam et al. 2011) have been reported for effective CTC isolation. For others utilizing biological properties, the immunointeraction between CTCs and bio-functionalized microstructures (Nagrath et al. 2007; Stott et al. 2010; Kralj et al. 2012; Andree et al. 2016; Gleghorn et al. 2010; Zhang et al. 2016) or magnetic beads (Min et al. 2015; Kang et al. 2012; Kim et al. 2013) has been extensively explored and implemented for CTC isolation. A few integrated analytical systems, such as IsoFlux and CellSearch, have been commercialized and able to realize semiautomated isolation and analysis of CTCs (Wang et al. 2013; Lopez-Riquelme et al. 2013).

For the bioaffinity-based methods, it is a critical strategy to enhance the interaction between tumor cells and the bio-functionalized substrates, making use of local microvortex, enlarged effective contact area, elongated time of interaction or other important spatiotemporal factors. Previously, a high-throughput microfluidic device with unique herringbone structure was firstly designed and fabricated for efficient CTC isolation. Local microvortex was induced by the special design of herringbone structure to increase the conjugation between target CTCs and the antibody-modified channel surface based on cell affinity chromatography (Stott et al. 2010; Deng et al. 2014; Xue et al. 2014). The highest capture rate of PC3 tumor cells can reach up to ~80% at the concentration of 1000 cells mL$^{-1}$. CTCs were found in 14 out of 15 patients with metastatic cancer showing an average frequency of 386 $\pm$ 238 CTCs mL$^{-1}$. For clinical applications, molecular and genetic characterizations of the captured CTCs can provide critical evidence for disease prognosis and elucidating the therapeutic regimen to suppress cancer progression (Yeo et al. 2016; Arya et al. 2013). Additionally, monitoring the post-therapy CTC level can also contribute to identifying ineffective treatments and invalid prognosis (Li et al. 2016; Caceres et al. 2015). However, most existing devices cannot reversibly retrieve captured tumor cells due to the strong immunoreaction between the antigens expressed on the cell membrane and the antibody coupled on the substrates.

In this work, a dual-functional microchip with double parallel layer of herringbone structure was designed and fabricated to achieve efficient CTC isolation and retrieval. Hep3B hepatocellular carcinoma cell line was selected as the CTC model, which overexpresses epithelial cell adhesion molecule (EpCAM) on the cell membrane (Yamashita et al. 2009). The microchip made of polydimethylsiloxane (PDMS) was following traditional soft lithography method. The internal channel surface was covalently linked with anti-EpCAM for CTC capture. The cell suspension containing Hep3B cells under specific concentration was introduced into the chip using a digital pump that precisely controls the infusing rate. After immunoreaction, the capture efficiency was calculated based on fluorescence imaging. D-biotin was then introduced into the channel as a competitive inhibitor to replace the active binding site of DSB-X biotinylated anti-EpCAM, and thus the captured CTCs were released from the binding site for subsequent collection (Hirsch et al. 2002). Both experimental and simulation results demonstrated that double parallel layers of herringbone structure can significantly enhance CTC capture attributed to the synergistic increase in both contact surface and local vortex. The superior CTC isolation and elution performance was also demonstrated under various cell concentrations and sample perfusion rates, indicating its good potential for fast and efficient CTC harvesting for cancer diagnosis and therapy.

## 2 Materials and methods

### 2.1 Materials

Polydimethylsiloxane SYLGARD 184 silicone elastomer kit was obtained from Dow Corning Inc., USA. Negative photoresist SU-8 2025 and SU-8 developer was supplied by Microchem Corp., USA. Soda lime photomask with herringbone pattern was printed by Bonda Technology Pte. Ltd., Singapore. Chemicals for antibody modification: 3-mercaptopropyl trimethoxysilane (3-MPS, 95%), $N$-$\gamma$-maleimidobutyryloxy succinimide ester (GMBS, $\geq$98%), bovine serum albumin (BSA, $\geq$98%), and ethanol ($\geq$99.8) were obtained from Sigma-Aldrich, Singapore. NeutrAvidin biotin-binding protein was purchased from Fisher Scientific, Singapore. Antihuman EpCAM was provided by Biomed Diagnostic, Singapore. Reagents for cell culture: Dulbecco's modified Eagle's medium (DMEM), fetal bovine serum (FBS), penicillin/streptomycin, D-biotin, CFDA SE cell tracer kit, and 1$\times$ PBS (pH = 7.4) were provided by Life Technologies, Singapore.

### 2.2 Device design

As shown in Fig. 1a, the device is composed of one inlet, one outlet, and eight working channels with double parallel layers of herringbone structure. The height of herringbone structure in both layers is 45 $\mu$m, and the overall height of channel is 115 $\mu$m. The widths of chevron structure and gap between neighbor herringbones are both 50 $\mu$m. The
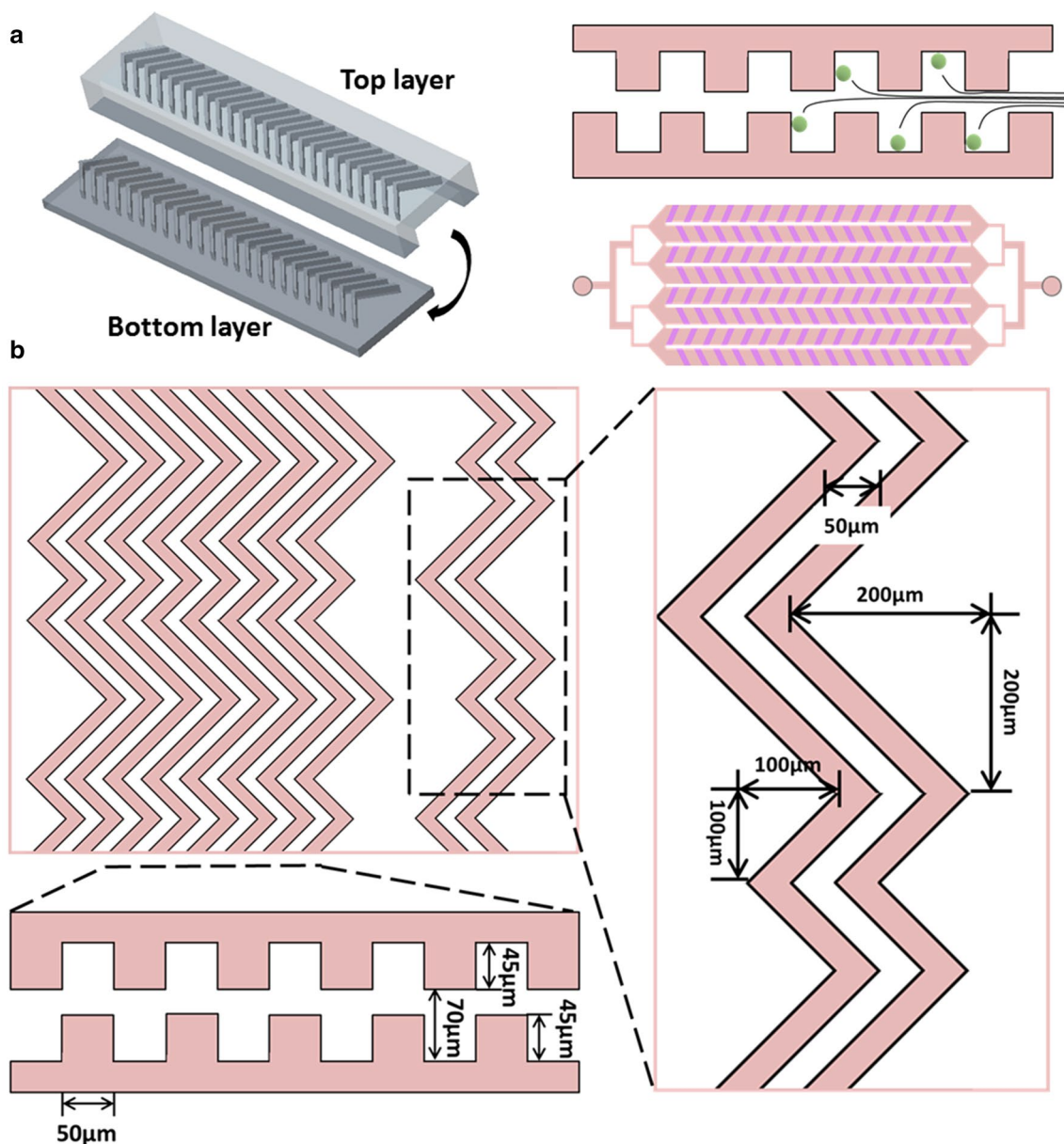
**Fig. 1** **a** Schematic illustration of three-dimensional (3D) structure of the device with double layers of herringbone structure and CTC capture based on cell surface immunoreaction, **b** geometric dimensions of the device in horizontal and vertical cross sections

angle between the herringbone slop direction and main channel axis is set as 45°. Double layers of herringbone structure with alternative permutation grooves are designed to induce significant local vortex to enhance micromixing and to increase total contact area for CTC capture. Geometric dimensions of the device are shown in Fig. 1b in horizontal and vertical cross sections.

### 2.3 Device fabrication

Double layers of PDMS slices with herringbone structure were fabricated for device assembly. Briefly, masters with

desirable height of features were fabricated by patterning negative photoresist SU-8 2025 on silicon wafer using photolithographic method. PDMS slice was prepared by pouring PDMS elastomer base mixed with curing agent by weight ratio of 10:1 onto the master mold. After degassing and curing in an oven at 70 °C for 4 h, the PDMS replica was carefully removed from the mold (Friend and Yeo 2010). The two PDMS layers were cut with exact dimensions to facilitate the alignment and assembly of the final device. After brief oxygen plasma treatment, the bottom PDMS layer was firstly bonded with a glass slide (1 in. × 3 in.) that worked as a supporting base of the entire

**Fig. 2** Scheme of procedures to immobilize antibody on channel surface
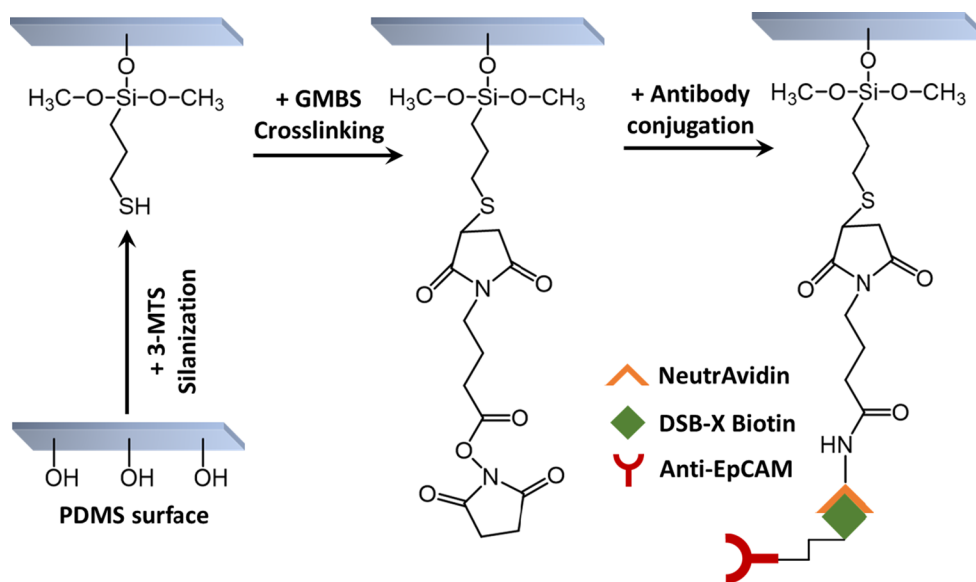


chip. Then, the microchannels were constructed by precisely aligning the top PDMS layer with the bottom PDMS layer under an optical microscope.

## 2.4 Functionalization of microchannel with Anti-EpCAM

To modify the channel surface with antibody, the device interior was firstly incubated with 4% (v/v) of 3-MPTS dispersed in ethanol for 1 h at 25 °C. After washing with ethanol thrice, the chip was treated with 10 mM of GMBS dispersed in ethanol for 30 min at room temperature. Then, the chip was washed with ethanol thrice, followed by treatment with 10 μg mL$^{-1}$ NeutrAvidin dispersed in PBS for 1 h in ambient environment. Afterward, channels were filled with 20 μg mL$^{-1}$ DSB-X biotinylated anti-EpCAM solution in PBS containing 1% (w/v) BSA, and further incubated for 1 h at room temperature. The unbounded antibody after reaction was removed by thoroughly washing the device with PBS. Finally, the device was ready for experiments in 24 h. Figure 2 shows the procedures to immobilize the antibody on channel surface.

## 2.5 Cell culture

Hep3B cells were expanded using DMEM supplemented with 10% FBS and a mixture of penicillin (100 U mL$^{-1}$)/ streptomycin (100 μg mL$^{-1}$). Cells were seeded in a culture flask under a humidified atmosphere with 5% CO$_2$ at 37 °C. The non-adherent cells were removed after overnight incubation, and the attached cells were further expanded until reaching 80% of confluence with media changed every 2–3 days. To harvest the cells with good

purity for microfluidic test, cell suspension was prepared using 0.25% EDTA–trypsin before use.

## 2.6 Microfluidic capture and retrieving CTCs

As shown in Fig. 3, the experiment was performed with the integrated platform consisting of cell staining unit, microchip core testing unit, and waste collection unit, which were arranged in serial. A digital pump system (Legato 180, KD Scientific, MA, USA) was used to introduce the sample solution into the chip with precisely controllable flow rate. Hep3B cells were firstly stained with CFDA SE fluorescent dye, and cell density was counted using Moxi Z mini automated cell counter (ORFLO Technologies, USA). Afterward, the sample was prepared by spiking specific number of cells into 1 mL of 1× PBS and was pumped into the device at various flow rates of 1, 1.5, and 2 mL h$^{-1}$, respectively. To prevent cells from precipitating in the syringe, a magnetic stirrer was placed in each syringe and an external magnetic field was applied to gently mix the sample periodically (~10-min intervals). A subsequent rinsing step was conducted to remove unbound cells from the chip by flowing 1× PBS at 4 mL h$^{-1}$ for 15 min. The number of captured cells was counted manually using a fluorescence microscope (IX71, Olympus, Singapore). The capture efficiency was calculated as the number of captured cells in the device divided by the total number of spiked cells flowed through the channel. For retrieving CTCs after capture, 10 mM of D-biotin was infused into the chip to release the cells from interior channel walls. The reaction was allowed to proceed for 30 min, followed by harvesting dissociated CTCs through washing with PBS thoroughly. The cell elution rate was evaluated based on the relative ratio between

**Fig. 3** Illustration of experimental procedures on CTC capture
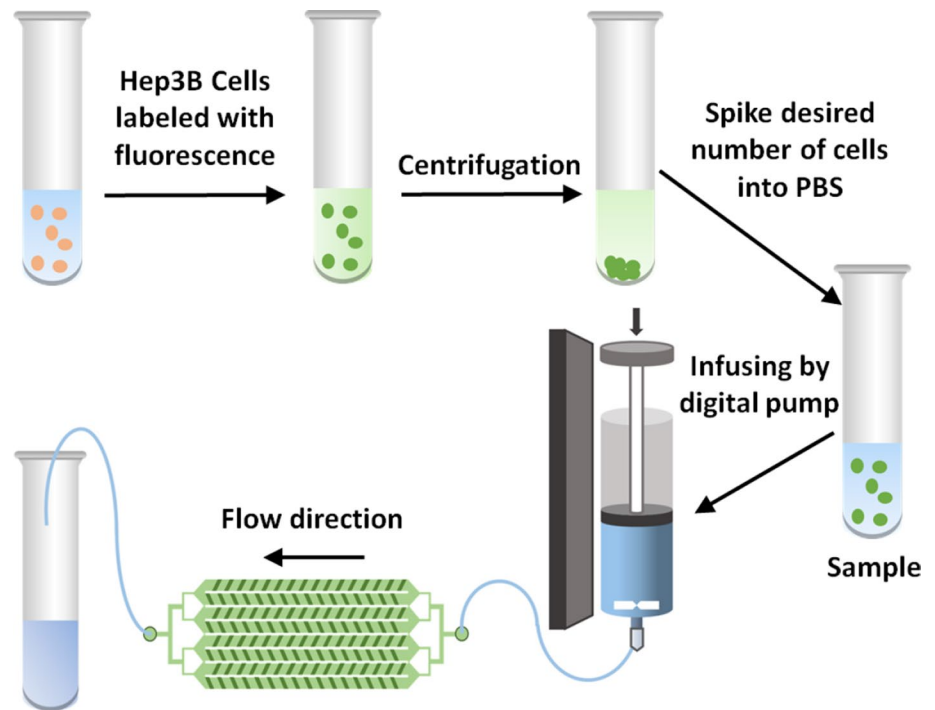


the number of CTCs retrieved from the device and overall CTC captured before elution.

# 3 Results and discussion

## 3.1 Numerical simulation of fluid flow in the microchannel

Because the flow behavior in the microchannel directly determines the cell surface interaction, a finite element-based simulation was conducted to study the flow regime using COMSOL Multiphysics 4.3a (COMSOL, Inc., USA). The governing equations and boundary conditions for the simulation are defined as follows.

Since the flow is driven by pressure only, the steady-state Navier–Stokes equation for incompressible flow is used.

$$\rho \frac{\partial \vec{u}}{\partial t} + \rho \vec{u} \cdot \nabla \vec{u} = -\nabla P + \eta \nabla^2 \vec{u} \tag{1}$$

Continuity equation:

$$\nabla \cdot \vec{u} = 0 \tag{2}$$

Boundary conditions:

$$\text{Channel walls} : \vec{u} = 0, \vec{n} \cdot \nabla P = 0 \tag{3a}$$

$$\text{Inlet} : v = 76 \ \mu\text{m s}^{-1} \tag{3b}$$

$$\text{Outlet} : P = 0 \tag{3c}$$

where $\vec{u}$ denotes flow velocity; $P$ is the pressure; $\eta$ is the fluid viscosity; $\rho$ is the fluid density.

In Fig. 4a, a typical fraction of microchannel (2 mm length and 1.2 mm width) was selected to show the computational domain in this proof-of-concept simulation study. The inflow rate was defined as 76 $\mu$m s$^{-1}$, which was consistent with the perfusion velocity of 1 mL h$^{-1}$. From the simulation results of flow streamlines (Fig. 4b), a unique flow pattern in both herringbone layers was observed, which was deviated from the main flow direction in the middle layer of the channel. Particularly, the main flow near the herringbone ceiling and floor was split into subordinate flows confined in the grooves periodically, where they were recombined into the main flow at the groove end. In this way, tumor cells experienced a comparatively longer distance in herringbone grooves than in the flows of main channel. The average flow rate was 21 $\mu$m s$^{-1}$ in the herringbone groove as compared to 208 $\mu$m s$^{-1}$ in the main channel (Fig. 4c). The slow flow rate in the grooves facilitated the immunoreaction efficiency between CTCs and functionalized channel walls. Meanwhile, the results indicated that the tumor cells flowing close to the herringbone grooves had more opportunities to be drawn into these grooves due to the local microvortex. Moreover, the design of double layers of herringbone grooves dramatically enlarged the total internal area of the chip compared to the flat channel or design of single herringbone layer. Therefore, the synergistic effects of increased contact area, slow velocity in herringbone grooves, enhanced local microvortex, and elongated flow distance contributed to the
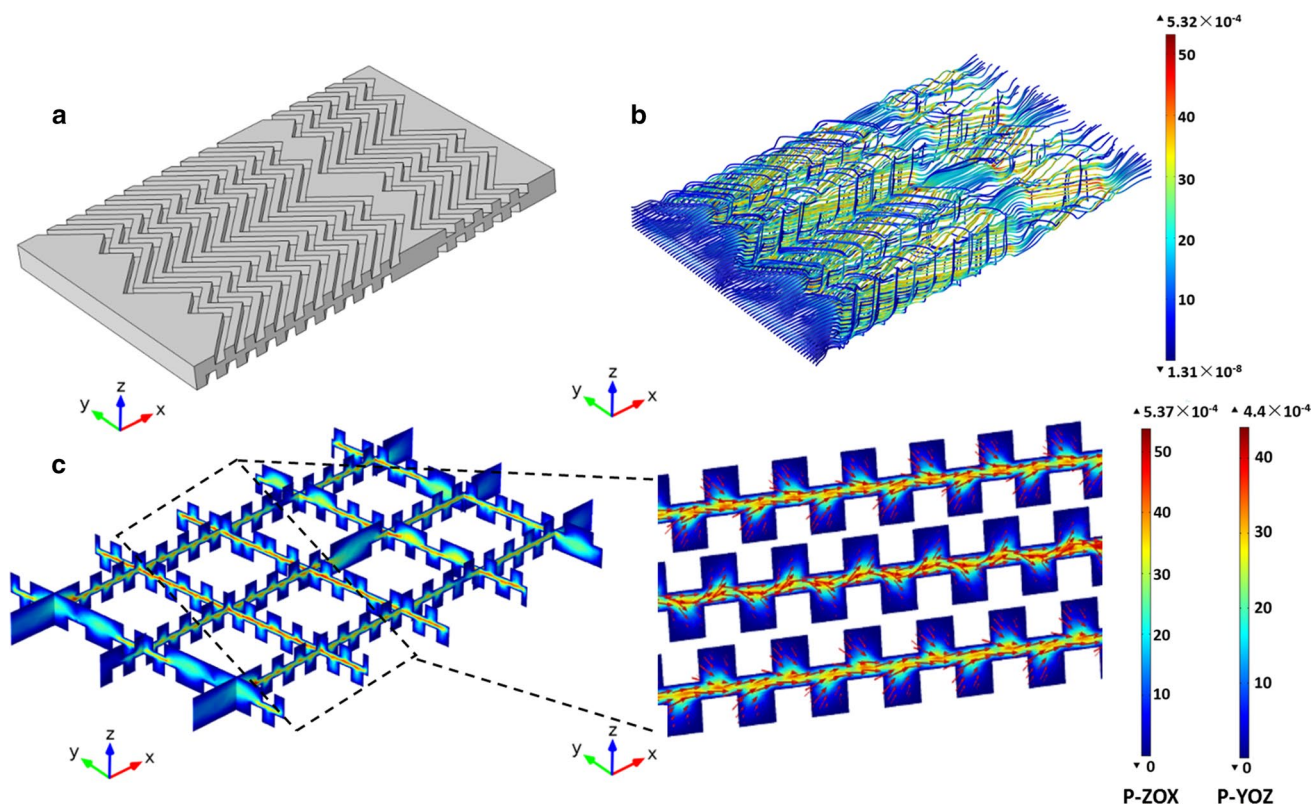
**Fig. 4** Numerical simulations of the flow pattern in the channel: **a** 3D geometric structure of the computation domain, **b** 3D flow streamlines, **c** 2D velocity field simulated in stacked cross section of *ZOX* and *YOZ* planes at multiple positions

enhanced immunoreaction and a higher CTC binding efficiency on the microchannel surface.

## 3.2 Evaluating the performance of device on CTC capture and retrieving

The captured CTCs were imaged using microscopy in bright field and dark field. For fluorescence imaging in dark field, the CTCs were labeled with CFDA SE, which can diffuse into cytoplasm and bind with intracellular amine sources emitting observable green fluorescence. This dye results in minimum cell death under the concentration of 10 μM and is a very common long-term cell tracer used in vitro and in vivo to determine whether a cell is proliferating. After introducing the sample spiked with $1 \times 10^4$ CTCs at flow rate of 1 mL h$^{-1}$, images of the captured CTCs were recorded as shown in Fig. 5a, b. The green dots in the fluorescence image indicated the viable CTCs that were corresponding to those captured at the same position under bright field. The green fluorescence of the tumor cells captured on the chip (Fig. 5) indicated that most of the retrieved cells maintained good viability. To evaluate the retrieving efficiency after elution step, a group of microscopic images were recorded to show the remaining

bounded cells as shown in Fig. 5c, d. Obviously, only a few CTCs were still attached on the channel surface after elution, while most isolated CTCs were dissociated from the binding sites and collected at the outlet.

The device performance on the CTC capture efficiency was evaluated by processing samples with spiked CTCs under different infusion rates. As shown in Fig. 6, flow rate played a critical role to influence CTC capture efficiency because it determined the time of cell surface interaction. Under the relatively lower flow rate of 1 mL h$^{-1}$, the CTC capture efficiency reached up to 75% with the cell number density ranging from 10 to $10^4$ mL$^{-1}$, indicating a broad dynamic range of target cell concentration. In the presence of higher CTC concentration level of $10^4$ mL$^{-1}$, the capture rate reduced to 50.2% only, which could be due to the saturated binding sites on the surface of microchannel. However, for regular clinical CTC concentration ranges of 100, 50, and 10 mL$^{-1}$, the capture efficiency for Hep3B cells was 76.4, 85, and 90%, respectively. Prior work reported the highest capture rate of 65% for NSC lung cancer cells (100 mL$^{-1}$ spiked in PBS) using a chip patterned with microposts (Nagrath et al. 2007), and 89% for PC3 prostate cancer cells (100 mL$^{-1}$ spiked in blood) using a chip patterned with a single layer of herringbone
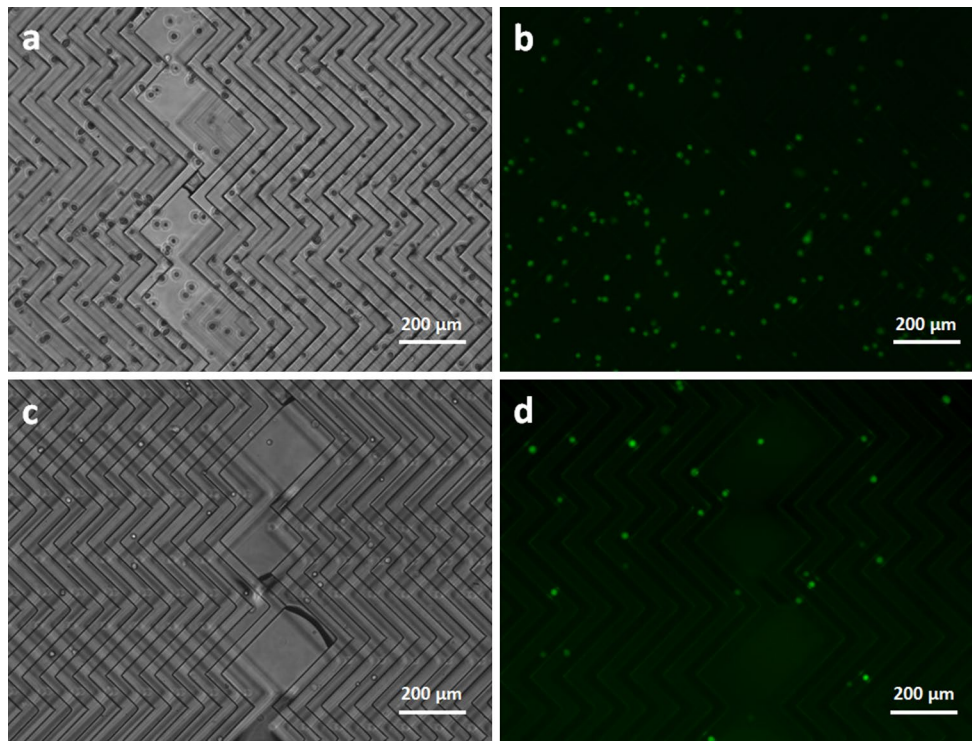
**Fig. 5** Microscopic images: **a** bright-field imaging and **b** fluorescence imaging of the captured CTCs, **c** bright-field imaging and **d** fluorescence imaging of the remaining CTCs after elution
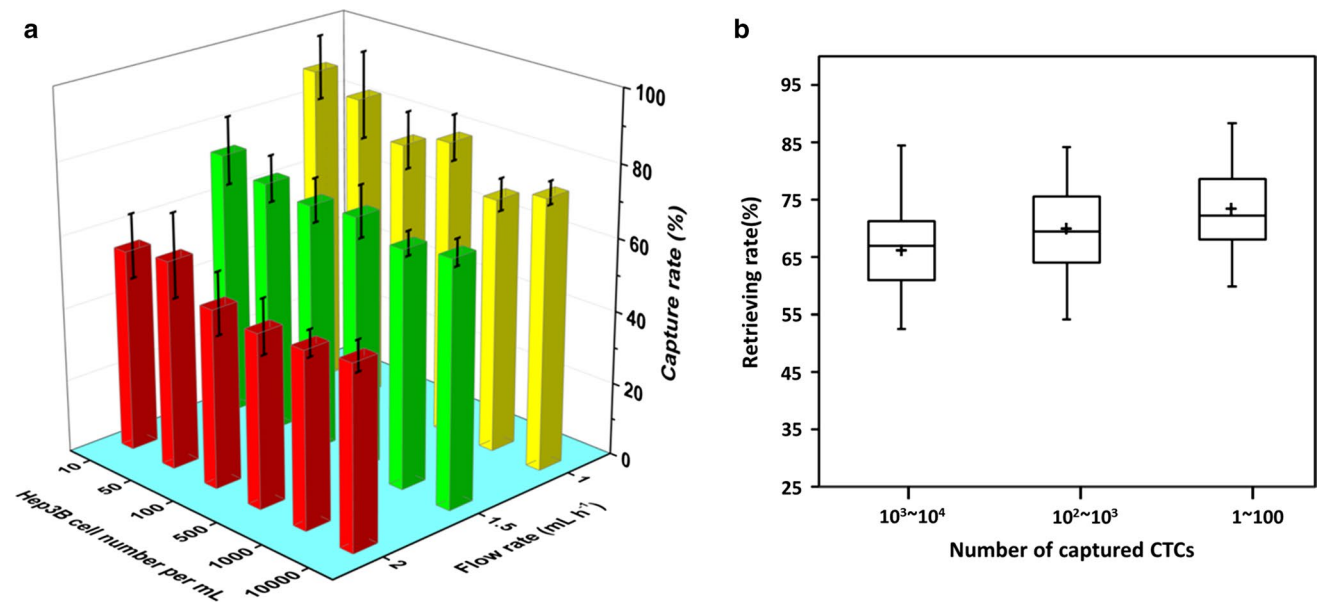


**Fig. 6 a** 3D column bar chart showing the capture rate of CTCs spiked in PBS with various cell number densities from 10 to $10^4$ $mL^{-1}$ and flow rate from 1 to 2 mL $h^{-1}$, respectively ($n = 4$), **b** mean and median of retrieving rate of CTCs illustrated by *box* and *Whiskers plots* ($n = 10$). Means are represented by *plus sign*

structure (Stott et al. 2010). Although the CTC capture efficiency is also dependent on the cell type and viability, our device has exhibited similar performance as compared to other reported devices in the literature. The high capture efficiency was attributed to the double layers of herringbone structure, which achieved a promising

sensitivity for clinical use with the detection limit down to 10 CTCs mL$^{-1}$. The overall isolation procedure could be accomplished within 1 h for processing 1 mL of sample. Under the higher flow rate of 1.5 and 2 mL h$^{-1}$, the average capture efficiency reduced to 68 and 52%, respectively. The inferior CTC binding capability under higher flow rates was due to the decreased time of cell surface interaction and increased flow shear that prevented cell attachment.

For retrieving CTCs, D-biotin was applied to competitively occupy the active binding sites on NeutrAvidin and the captured CTCs were dissociated and released from the device. As shown in Fig. 6b, the retrieving rate of CTCs reached up to 68% in the range of 10$^2$–10$^4$ captured CTC, indicating the excellent performance of D-biotin to dissociate the bound CTCs. The average CTC retrieving rate achieved was 73.4% with cell number density from 1 to 100 mL$^{-1}$ that was more clinically relevant. The captured CTCs can be efficiently retrieved using such platforms for further analyses. In addition to capture and retrieval of CTCs, other important functions such as on-chip culture and in situ molecular analysis of CTCs are expected for the next generation of integrated CTC analyzer (Green et al. 2016).

## 4 Conclusion

A dual-functional microfluidic chip with double parallel herringbone layers was designed and fabricated for efficient isolation and retrieval of CTCs. Anti-EpCAM was covalently conjugated to the channel surface for CTC capture. The double layers of herringbone structure significantly increased the inner surface area and induced local microvortex, which enhanced the cell–substrate interaction. The capture efficiency of CTCs obtained using this device was remarkably improved compared to previous studies. Furthermore, the captured CTCs can be successfully retrieved from the device for downstream cellular and molecular analyses by introducing D-biotin to block the active binding sites of antibody. Such platform has a good potential for developing the new generation of integrated devices for CTC searching and analyses.

## References

Alazzam A, Stiharu I, Bhat R et al (2011) Interdigitated comb-like electrodes for continuous separation of malignant cells from blood using dielectrophoresis. Electrophoresis 32:1327–1336

Alix-Panabieres C, Pantel K (2014) Challenges in circulating tumour cell research. Nat Rev Cancer 14:623–631

Andree KC, Barradas AMC, Nguyen AT et al (2016) Capture of tumor cells on anti-EpCAM-functionalized poly(acrylic acid)-coated surfaces. ACS Appl Mater Interfaces 8:14349–14356

Arya SK, Lim B, Rahman AR (2013) Enrichment, detection and clinical significance of circulating tumor cells. Lab Chip 13:1995–2027

Balic M, Williams A, Lin H et al (2013) Circulating tumor cells: from bench to bedside. Annu Rev Med 64:31–44

Barok M, Szollosi J (2011) Steps in metastasis research: analyzing, collecting, and culturing circulating tumor cells. Cytom Part A 79:93–94

Bernards R, Weinberg RA (2002) Metastasis genes: a progression puzzle. Nature 418:823

Caceres G, Puskas JA, Magliocco AM (2015) Circulating tumor cells: a window into tumor development and therapeutic effectiveness. Cancer Control 22:167–176

den Toonder J (2011) Circulating tumor cells: the Grand Challenge. Lab Chip 11:375–377

Deng Y, Zhang Y, Sun S et al (2014) An integrated microfluidic chip system for single-cell secretion profiling of rare circulating tumor cells. Sci Rep UK 4:7499

Devriese LA, Bosma AJ, van de Heuvel MM et al (2012) Circulating tumor cell detection in advanced non-small cell lung cancer patients by multi-marker QPCR analysis. Lung Cancer 75:242–247

Friend J, Yeo L (2010) Fabrication of microfluidic devices using polydimethylsiloxane. Biomicrofluidics 4:026502

Gascoyne PR, Shim S (2014) Isolation of circulating tumor cells by dielectrophoresis. Cancers 6:545–579

Giuliano M, Giordano A, Jackson S et al (2014) Circulating tumor cells as early predictors of metastatic spread in breast cancer patients with limited metastatic dissemination. Breast Cancer Res 16:440

Gleghorn JP, Pratt ED, Denning D et al (2010) Capture of circulating tumor cells from whole blood of prostate cancer patients using geometrically enhanced differential immunocapture (GEDI) and a prostate-specific antibody. Lab Chip 10:27–29

Gorges TM, Pantel K (2013) Circulating tumor cells as therapy-related biomarkers in cancer patients. Cancer Immunol Immunother 62:931–939

Green BJ, Safaei TS, Mepham A et al (2016) Beyond the capture of circulating tumor cells: next-generation devices and materials. Angew Chem Int Edit 55:1252–1265

Hirsch JD, Eslamizar L, Filanoski BJ et al (2002) Easily reversible desthiobiotin binding to streptavidin, avidin, and other biotin-binding proteins: uses for protein labeling, detection, and isolation. Anal Biochem 308:343–357

Hosokawa M, Arakaki A, Takahashi M et al (2009) High-density microcavity array for cell detection: single-cell analysis of hematopoietic stem cells in peripheral blood mononuclear cells. Anal Chem 81:5308–5313

Kang JH, Krause S, Tobin H et al (2012) A combined micromagnetic-microfluidic device for rapid capture and culture of rare circulating tumor cells. Lab Chip 12:2175–2181

Kim S, Han SI, Park MJ et al (2013) Circulating tumor cell microseparator based on lateral magnetophoresis and immunomagnetic nanobeads. Anal Chem 85:2779–2786

Kralj JG, Arya C, Tona A et al (2012) A simple packed bed device for antibody labelled rare cell capture from whole blood. Lab Chip 12:4972–4975

Li Y, Gong J, Zhang Q et al (2016) Dynamic monitoring of circulating tumour cells to evaluate therapeutic efficacy in advanced gastric cancer. Brit J Caner 114:138–145

Lopez-Riquelme N, Minguela A, Villar-Permuy F et al (2013) Imaging cytometry for counting circulating tumor cells: comparative

analysis of the Cell Search vs ImageStream systems. Apmis 121:1139–1143

Min H, Jo SM, Kim HS (2015) Efficient capture and simple quantification of circulating tumor cells using quantum dots and magnetic beads. Small 11:2536–2542

Morimoto A, Mogami T, Watanabe M et al (2015) High-density dielectrophoretic microwell array for detection, capture, and single-cell analysis of rare tumor cells in peripheral blood. PLoS ONE 10:e0130418

Nagrath S, Sequist LV, Maheswaran S et al (2007) Isolation of rare circulating tumour cells in cancer patients by microchip technology. Nature 450:1235–1239

Norton L, Massague J (2006) Is cancer a disease of self-seeding? Nat Med 12:875–878

Stott SL, Hsu CH, Tsukrov DI et al (2010) Isolation of circulating tumor cells using a microvortex-generating herringbone-chip. Proc Natl Acad Sci USA 107:18392–18397

Sun JS, Li M, Liu C et al (2012) Double spiral microchannel for label-free tumor cell separation and enrichment. Lab Chip 12:3952–3960

Tang YD, Shi J, Li SS et al (2014) Microfluidic device with integrated microfilter of conical-shaped holes for high efficiency and high purity capture of circulating tumor cells. Sci Rep UK 4:6052

Tsai WS, Chen JS, Shao HJ et al (2016) Circulating tumor cell count correlates with colorectal neoplasm progression and is a prognostic marker for distant metastasis in non-metastatic patients. Sci Rep UK 6:24517

Valastyan S, Weinberg RA (2011) Tumor metastasis: molecular insights and evolving paradigms. Cell 147:275–292

van de Stolpe A, Pantel K, Sleijfer S et al (2011) Circulating tumor cell isolation and diagnostics: toward routine clinical use. Cancer Res 71:5955–5960

Wang LX, Asghar W, Demirci U et al (2013) Nanostructured substrates for isolation of circulating tumor cells. Nano Today 8:374–387

Wang J, Lu W, Tang C et al (2015) Label-free isolation and mrna detection of circulating tumor cells from patients with metastatic lung cancer for disease diagnosis and monitoring therapeutic efficacy. Anal Chem 87:11893–11900

Warkiani ME, Khoo BL, Wu LD et al (2016) Ultra-fast, label-free isolation of circulating tumor cells from blood using spiral microfluidics. Nat Protoc 11:134–148

Xue P, Ye K, Gao J et al (2014) Isolation and elution of Hep3B circulating tumor cells using a dual-functional herringbone chip. Microfluidics Nanofluidics 16:605–612

Yamashita T, Ji J, Budhu A et al (2009) EpCAM-positive hepatocellular carcinoma cells are tumor-initiating cells with stem/progenitor cell features. Gastroenterology 136:1012–1024

Yeo T, Tan SJ, Lim CL et al (2016) Microfluidic enrichment for the single cell analysis of circulating tumor cells. Sci Rep UK 6:22076

Yu M, Bardia A, Aceto N et al (2014) Ex vivo culture of circulating breast tumor cells for individualized testing of drug susceptibility. Science 345:216–220

Zetter BR (1998) Angiogenesis and tumor metastasis. Annu Rev Med 49:407–424

Zhang FL, Jiang Y, Liu X et al (2016) Hierarchical nanowire arrays as three-dimensional fractal nanobiointerfaces for high efficient capture of cancer cells. Nano Lett 16:766–772